

Implications of the muon anomalous magnetic moment in a Doublet Left-Right Symmetric Model

M. Zeleny-Mora^{1*}, R. Gaitán-Lozano^{1†}, R. Martínez^{2‡}

¹Departamento de Física, FES-Cuautitlán, UNAM, C.P. 54770, Estado de México, México.

²Departamento de Física, Universidad Nacional de Colombia, K. 45 No. 26-85, Bogotá, Colombia.

March 31, 2026

Abstract

We compute the complete set of one-loop contributions to the muon anomalous magnetic moment, $a_\mu = (g-2)_\mu/2$, in the Doublet Left-Right Symmetric Model (DLRSM), based on the gauge group $SU(2)_L \otimes SU(2)_R \otimes U(1)_{B-L}$ with neutrino masses generated via the inverse seesaw (ISS) mechanism. We evaluate all four one-loop topologies—VFF, SFF, FVV, and FSS—arising from the extended gauge bosons (W' , Z'), the new scalar sector (H_3^0 , A_1^0 , H_R^\pm , H_L^\pm), and the heavy neutrino spectrum generated by the ISS mechanism, using the Casas-Ibarra parametrization to express the neutrino mixing in terms of physical observables. Imposing the experimental bound on Δa_μ , we establish that $v_R \lesssim 1$ TeV is excluded, implying lower bounds $m_{W'} \gtrsim 325$ GeV, $m_{Z'} \gtrsim 385$ GeV, and $m_N \gtrsim 700$ GeV under the manifest left-right symmetry condition $g_R = g_L$. Relaxing this condition to $g_R \neq g_L$ strengthens the gauge boson bounds to $m_{W'} \gtrsim 1625$ GeV and $m_{Z'} \gtrsim 1650$ GeV.

1 Introduction

The Standard Model (SM) of particle physics has been remarkably successful in describing fundamental interactions at the electroweak scale. Nonetheless, several open questions remain, including the origin of neutrino masses, the nature of parity violation, and the existence of lepton flavor violation (LFV). In fact, neutrino oscillation experiments confirm that neutrinos have nonzero masses, and therefore a new mass generation mechanism is needed to describe this small scale. An accepted explanation is the type-I seesaw mechanism which introduces right-handed neutrinos ν_R and heavy Majorana neutrinos with mass matrix M_R , for three right-handed neutrino generations one obtains a 6×6 full neutrino mass matrix \mathcal{M}_ν . In the limit $|m_D| \ll |M_R|$, the light neutrino mass matrix $\mathcal{M}_{\text{light}}$ is approximately

$$\mathcal{M}_{\text{light}} \approx -m_D^\top M_R^{-1} m_D.$$

where m_D is the Dirac mass matrix. Typically, this requires $M_R \approx 10^{14}$ GeV, a scale beyond current experimental reach. The inverse seesaw (ISS) mechanism offers an alternative by introducing three pairs of fermionic singlets (N_R, S) . In addition to M_R a new small Majorana mass matrix μ_S for the singlets S is included. Assuming the hierarchy $|\mu_S| \ll |m_D| \ll |M_R|$, the light neutrino mass matrix is approximated as follows

$$\mathcal{M}_{\text{light}} \approx m_D^\top M_R^{-1} \mu_S (M_R^\top)^{-1} m_D,$$

allowing right-handed neutrinos to reside at the TeV scale, potentially within reach of current collider experiments.

The Left-Right Symmetric Model (LRSM) offers a compelling framework to address parity violation by extending the SM gauge group to

$$SU(3)_C \otimes SU(2)_L \otimes SU(2)_R \otimes U(1)_{B-L},$$

restoring left-right symmetry at higher energies [1, 2, 3, 4]. In contrast to the canonical version based on triplet scalar fields and neutrino masses described by the seesaw type I or II, the Doublet Left-Right Symmetric Model (DLRSM) introduces a scalar sector consisting of a bidoublet Φ and two doublets χ_L and χ_R , which simplifies the

*moiseszeleny@gmail.com

†regaitan@gmail.com

‡remartinez@unal.edu.co

scalar potential[5] and allows the incorporation of ISS mechanism to generate light neutrino masses with right-handed neutrinos at TeV scale [6, 7]. At hadron colliders, the canonical production signature of such TeV-scale states is the Keung--Senjanovic (KS) process, $pp \rightarrow W'^{\pm} \rightarrow \ell^{\pm} N \rightarrow \ell^{\pm} \ell^{\pm} jj$, in which an on-shell W' decays to a charged lepton and a heavy Majorana neutrino, yielding a same-sign dilepton plus dijet final state, this constitutes a distinctive signature of lepton-number violation at colliders [8].

The symmetry-breaking scale v_R of the LRSM is already tightly constrained from the quark flavor sector. Indirect CP violation in the neutral kaon system via the chromomagnetic dipole operator, which receives a GIM-enhanced coefficient of order $10^5 \zeta$ relative to the SM contribution, implies a lower bound $M_{W'} \gtrsim 2.8 - 3$ TeV on the right-handed gauge boson mass for phenomenologically viable phase configurations [9]. A comprehensive analysis of $\Delta F = 2$ transitions in the K , B_d and B_s meson systems including one-loop self-energy and vertex renormalization diagrams required for a gauge-independent result shows that B -meson oscillation data place constraints competitive with those from kaon physics, yielding an absolute lower bound $M_{W'} \gtrsim 2.9 - 3.1$ TeV at 95% CL [10]. Complementary to these quark-sector bounds, precision lepton observables such as the anomalous magnetic moment of the muon, $a_{\mu} = (g - 2)_{\mu}/2$, probe the LRSM parameter space through a different set of loop topologies.

The present world average synthesizes two decades of precision measurements. The BNL E821 experiment provided the first high-precision determination, establishing a long-standing discrepancy of approximately 3.7σ with the then-current SM prediction [11]. The Fermilab E989 experiment subsequently confirmed and sharpened this result in three successive campaigns: Run 1 at 0.46 ppm [12], Runs 2 – 3 at 0.20 ppm [13], and the final combination of all six runs at an unprecedented 127 ppb [14] a fourfold improvement over BNL and the most precise measurement of a_{μ} ever achieved.

Recently, experimental searches for the anomalous magnetic moment of the muon $a_{\mu} = (g - 2)_{\mu}/2$ performed by Muon $g - 2$ Experiment at Fermi National Accelerator Laboratory (FNAL) has contributed to improve the world-average determination of [14]

$$a_{\mu}^{\text{exp}} = 1165920715 (145) \times 10^{-12}.$$

with an unprecedented precision of 127 ppb. The SM prediction of a_{μ} has recently been refined, with lattice-QCD providing a consolidated determination of the leading-order hadronic vacuum polarization at 0.9% precision. Incorporating this result yields [15],

$$a_{\mu}^{\text{SM}} = 116592033 (62) \times 10^{-11},$$

which agrees with the current experimental world average within uncertainties. Together, these results establish

$$\Delta a_{\mu} = a_{\mu}^{\text{exp}} - a_{\mu}^{\text{SM}} = (38 \pm 63) \times 10^{-11},$$

which implies no tension with the SM prediction at the current level of precision [15]. For Beyond the Standard Model (BSM) scenarios the new contributions to a_{μ} should be positive or negative but with a sufficiently small magnitude [16].

Motivated by these constraints, the implications of Δa_{μ} have been investigated in a broad class of gauge extensions of the SM. In the context of 331 models, which extend the electroweak gauge group to $SU(3)_C \otimes SU(3)_L \otimes U(1)$, a systematic examination of all one-loop topologies with neutral and charged scalar fields, singly and doubly charged gauge bosons, and neutral gauge bosons has been performed, showing that complementary electroweak, dark-matter, and collider constraints strongly restrict the symmetry breaking scale v_{χ} of these models [17]. In extensions with non-universal Abelian symmetries and an inverse seesaw neutrino sector, it has been found that the dominant positive contribution to Δa_{μ} originates from the SM W^+ boson interacting with exotic heavy Majorana neutrinos at one loop, while contributions from the extended neutral gauge sector and from the scalar sector are subleading or negative [18].

In this work, we compute all one-loop contributions to a_{μ} within the DLRSB, covering the four topologies VFF, SFF, FVV, and FSS arising from the extended neutral and charged gauge bosons (Z' and W'), the new scalar sector (H_3^0 , A_1^0 , H_R^{\pm} , H_L^{\pm}), and the heavy neutrino spectrum generated by the ISS mechanism. Using the experimental constraint on Δa_{μ} , we derive bounds on the right-handed symmetry-breaking scale v_R and the associated heavy-state mass spectrum. The paper is organized as follows. Section 2 describes the DLRSB gauge, scalar, and fermion sectors and establishes our notation. Section 3 presents the ISS mass matrix, its diagonalization, and the Casas-Ibarra parametrization used in our numerical scan. Section 4 derives the one-loop contributions to a_{μ} from each sector analytically. Section 5 presents the numerical analysis and the resulting constraints on the DLRSB parameter space. Section 6 summarizes our conclusions. The neutral gauge boson diagonalization and the complete set of master loop-integral formulas are collected in Appendices A and B, respectively.

2 The Doublet Left-Right Symmetric Model

The DLRSM realizes parity restoration at high energies by promoting the right-handed current to a full $SU(2)_R$ gauge interaction. The gauge group is

$$G_{\text{LR}} = SU(2)_L \otimes SU(2)_R \otimes U(1)_{B-L}, \quad (1)$$

augmented by a discrete parity symmetry \mathcal{P} that interchanges the L and R sectors [5]. The model reduces to the SM after two successive stages of spontaneous symmetry breaking (SSB):

$$G_{\text{LR}} \rightarrow SU(2)_L \otimes U(1)_Y \rightarrow U(1)_{\text{em}}. \quad (2)$$

The first breaking, driven by the VEV v_R of the right-handed doublet χ_R , generates masses for the heavy gauge bosons W' and Z' and for the right-handed neutrinos ν_R . The second breaking, driven by the bidoublet VEV k_1 , produces the SM fermion masses in the standard way.

2.1 Fermion content and charge assignments

Quarks and leptons are assigned to LR-symmetric doublet representations. Denoting the generation index by $i = 1, 2, 3$, the lepton and quark doublets and their gauge quantum numbers $(T_L, T_R, B - L)$ are

$$L_{iL} = \begin{pmatrix} \nu'_i \\ \ell'_i \end{pmatrix}_L : (2, 1, -1), \quad L_{iR} = \begin{pmatrix} \nu'_i \\ \ell'_i \end{pmatrix}_R : (1, 2, -1) \quad (3)$$

$$Q_{iL} = \begin{pmatrix} u'_i \\ d'_i \end{pmatrix}_L : (2, 1, 1/3), \quad Q_{iR} = \begin{pmatrix} u'_i \\ d'_i \end{pmatrix}_R : (1, 2, 1/3). \quad (4)$$

Under parity, the left and right fermion doublets interchange $\Psi_L \leftrightarrow \Psi_R$, for $\Psi = Q, L$.

The electric charge is given by the generalized Gell-Mann-Nishijima relation

$$Q = T_{3L} + T_{3R} + \frac{B - L}{2}.$$

To accommodate neutrino masses via the inverse seesaw mechanism (Section 3), we supplement the fermion content with three gauge-singlet fermions S_i ($i = 1, 2, 3$) which transform under parity as

$$S_i \longleftrightarrow S_i^c. \quad (5)$$

We adopt the Manifest Left-Right Symmetry (MLRS) condition $g_L = g_R \equiv g$, so the covariant derivatives acting on the fermion doublets are

$$D_\mu \Psi_L = \left(\partial_\mu - ig \frac{\vec{\tau}}{2} \cdot \vec{W}_{L\mu} - ig_{BL} \frac{(B-L)}{2} B_\mu \right) \Psi_L, \quad (6)$$

$$D_\mu \Psi_R = \left(\partial_\mu - ig \frac{\vec{\tau}}{2} \cdot \vec{W}_{R\mu} - ig_{BL} \frac{(B-L)}{2} B_\mu \right) \Psi_R. \quad (7)$$

After the second-stage breaking $SU(2)_R \otimes U(1)_{B-L} \rightarrow U(1)_Y$, the SM hypercharge is identified as $Y = T_{3R} + (B - L)/2$.

2.2 Scalar sector

The scalar sector consists of one bidoublet and two doublets,

$$\Phi(2, 2^*, 0), \quad \chi_L(2, 1, 1), \quad \chi_R(1, 2, 1) \quad (8)$$

with the parity assignments

$$\chi_L \longleftrightarrow \chi_R, \quad \Phi \longleftrightarrow \Phi^\dagger. \quad (9)$$

The field content is

$$\Phi = \begin{pmatrix} \phi_1^0 & \phi_1^+ \\ \phi_2^- & \phi_2^0 \end{pmatrix}; \quad \tilde{\Phi} = \sigma_2 \Phi^* \sigma_2, \quad \chi_{L,R} = \begin{pmatrix} \chi_{L,R}^+ \\ \chi_{L,R}^0 \end{pmatrix}_{L,R}, \quad (10)$$

and their VEVs are

$$\langle \Phi \rangle = \frac{1}{\sqrt{2}} \begin{pmatrix} k_1 & 0 \\ 0 & k_2 \end{pmatrix}, \quad \langle \chi_R \rangle = \frac{1}{\sqrt{2}} \begin{pmatrix} 0 \\ v_R \end{pmatrix}, \quad \langle \chi_L \rangle = \frac{1}{\sqrt{2}} \begin{pmatrix} 0 \\ v_L \end{pmatrix}. \quad (11)$$

Hereafter we set $k_2 = v_L = 0$, which eliminates $W - W'$ mixing (see Section 2.3) and simplifies the scalar mass spectrum.

The scalar potential consistent with the gauge symmetry and parity is [5]

$$V = V_\Phi + V_\chi + V_{\Phi\chi}, \quad (12)$$

with

$$\begin{aligned} V_\Phi = & -\mu_1^2 \text{Tr} \Phi^\dagger \Phi + \lambda_1 (\text{Tr} \Phi^\dagger \Phi)^2 \\ & + \lambda_2 \text{Tr} \Phi^\dagger \Phi \Phi^\dagger \Phi \\ & + \frac{1}{2} \lambda_3 \left(\text{Tr} \Phi^\dagger \tilde{\Phi} + \text{Tr} \tilde{\Phi}^\dagger \Phi \right)^2 \\ & + \frac{1}{2} \lambda_4 \left(\text{Tr} \Phi^\dagger \tilde{\Phi} - \text{Tr} \tilde{\Phi}^\dagger \Phi \right)^2 \\ & + \lambda_5 \text{Tr} \Phi^\dagger \Phi \tilde{\Phi}^\dagger \tilde{\Phi} \\ & + \frac{1}{2} \lambda_6 \left[\text{Tr} \Phi^\dagger \tilde{\Phi} \Phi^\dagger \tilde{\Phi} + \text{h.c.} \right], \end{aligned} \quad (13)$$

$$\begin{aligned} V_\chi = & -\mu_2^2 \left(\chi_L^\dagger \chi_L + \chi_R^\dagger \chi_R \right) \\ & + \rho_1 \left(\left(\chi_L^\dagger \chi_L \right)^2 + \left(\chi_R^\dagger \chi_R \right)^2 \right) \\ & + \rho_2 \chi_L^\dagger \chi_L \chi_R^\dagger \chi_R, \end{aligned} \quad (14)$$

$$\begin{aligned} V_{\Phi\chi} = & \alpha_1 \text{Tr} \Phi^\dagger \Phi \left(\chi_L^\dagger \chi_L + \chi_R^\dagger \chi_R \right) \\ & + \alpha_2 \left(\chi_L^\dagger \Phi \Phi^\dagger \chi_L + \chi_R^\dagger \Phi^\dagger \Phi \chi_R \right) \\ & + \alpha_3 \left(\chi_L^\dagger \tilde{\Phi} \tilde{\Phi}^\dagger \chi_L + \chi_R^\dagger \tilde{\Phi}^\dagger \tilde{\Phi} \chi_R \right). \end{aligned} \quad (15)$$

All parameters $\mu_{1,2}^2$, $\lambda_{1,2,3,4,5,6}$, $\rho_{1,2}$, and $\alpha_{1,2,3}$ are taken real, so that explicit CP violation is absent.

2.2.1 Physical scalar spectrum.

The scalar sector contains 16 real degrees of freedom from the fields Φ , χ_L and χ_R . After SSB, six are eaten by W , W' , Z , Z' leaving ten physical Higgs states. In the limit of $k_1 \ll v_R$ the mass eigenstates and their approximate masses are summarised in Table 1. We define

$$\begin{aligned} \alpha_{23} &= \alpha_2 - \alpha_3, & \alpha_{13} &= \alpha_1 + \alpha_3, \\ \lambda_{12} &= \lambda_1 + \lambda_2, & \rho_{21} &= \rho_2 - 2\rho_1, \\ \lambda_{2356} &= -\lambda_2 + 4\lambda_3 + \lambda_5 + \lambda_6, & \lambda_{2456} &= -\lambda_2 - 4\lambda_4 + \lambda_5 - \lambda_6. \end{aligned} \quad (16)$$

The neutral fields $\phi_{1,2}^0, \chi_{R,L}^0$ can be decomposed in terms of real and imaginary part, ($\phi \rightarrow (\langle \phi \rangle + \text{Re}(\phi) + i\text{Im}(\phi)) / \sqrt{2}$ with $\phi = \phi_{1,2}^0, \chi_{R,L}^0$). In the limit of $k_1 \ll v_R$, the two CP-even states mix according to

$$\begin{aligned} \text{Re}(\phi_1^0) &\approx \frac{k_1}{2\rho_1 v_R} \alpha_{13} H_2^0 + H_1^0, \\ \text{Re}(\chi_R^0) &\approx -\frac{k_1}{2\rho_1 v_R} \alpha_{13} H_1^0 + H_2^0, \end{aligned} \quad (17)$$

State	J^P	Role	Approximate mass ²
H_1^0	0^+	SM-like Higgs	$(2\lambda_{12} - \alpha_{13}^2/2\rho_1) k_1^2$
H_2^0	0^+	Heavy CP-even	$2\rho_1 v_R^2$
H_3^0	0^+	Heavy CP-even	$\frac{1}{2}\alpha_{23} v_R^2$
A_1^0	0^-	Heavy CP-odd	$\frac{1}{2}\alpha_{23} v_R^2$
H_4^0	0^+	Inert	$\frac{1}{2}\rho_{21} v_R^2$
A_2^0	0^-	Inert	$\frac{1}{2}\rho_{21} v_R^2$
H_R^\pm	0^\pm	Heavy charged	$\frac{1}{2}\alpha_{23} v_R^2$
H_L^\pm	0^\pm	Heavy charged	$\frac{1}{2}\rho_{21} v_R^2$

Table 1: Physical Higgs boson states and their leading-order masses in the limit $k_1 \ll v_R$.

where H_1^0 is identified with the SM Higgs and H_2^0 is a heavy neutral Higgs. The charged physical state H_R^\pm and the would-be Goldstone boson G_R^\pm arise from the mixing

$$\begin{aligned}\chi_R^\pm &\approx \frac{k_1 H_R^\pm}{v_R} + G_R^\pm, \\ \phi_1^\pm &\approx -\frac{k_1 G_R^\pm}{v_R} + H_R^\pm.\end{aligned}\tag{18}$$

The remaining physical states and their field identifications are

$$\begin{aligned}\text{Im}(\chi_L^0) &= A_2^0, & \phi_2^\pm &\approx G_L^\pm, \\ \text{Im}(\chi_R^0) &= G_{Z'}, & \chi_L^\pm &\approx H_L^\pm, \\ \text{Im}(\phi_1^0) &= G_Z, & \text{Re}(\phi_2^0) &\approx H_3^0, \\ \text{Im}(\phi_2^0) &= A_1^0, & \text{Re}(\chi_L^0) &\approx H_4^0.\end{aligned}\tag{19}$$

where G_L^\pm , G_Z and $G_{Z'}$ are the Goldstone bosons eaten by W , Z and Z' , respectively.

At leading order in v_R the states H_3^0 , A_1^0 and H_R^\pm are all degenerate with common mass $M^2 \approx \frac{1}{2}\alpha_{23} v_R^2$. Their mass splitting for H_3^0 and A_1^0 at order k_1^2 is controlled by

$$M_{H_3^0}^2 - M_{A_1^0}^2 = k_1^2 \delta^0, \quad \delta^0 \equiv \lambda_{2356} - \lambda_{2456},\tag{20}$$

and is negligible in the $k_1 \ll v_R$ employed in the numerical analysis, their contributions to a_μ nearly cancel each other in the limit $\delta^0 \rightarrow 0$. Similarly, H_4^0 and A_2^0 are exactly degenerate, however, they are inert with respect to the external lepton lines and do not contribute to a_μ .

2.3 Gauge sector

The kinetic Lagrangian for the scalar multiplets,

$$\mathcal{L}_D = (D_\mu \chi_L)^\dagger D_\mu \chi_L + (D_\mu \chi_R)^\dagger D_\mu \chi_R + \text{Tr} \left[(D_\mu \Phi)^\dagger D_\mu \Phi \right],$$

with

$$\begin{aligned}D_\mu \chi_L &= \partial_\mu \chi_L - \frac{i}{2} g \vec{\tau} \cdot \vec{W}_L \chi_L - \frac{i}{2} g_{B-L} B_\mu, \\ D_\mu \chi_R &= \partial_\mu \chi_R - \frac{i}{2} g \vec{\tau} \cdot \vec{W}_R \chi_R - \frac{i}{2} g_{B-L} B_\mu, \\ D_\mu \Phi &= \partial_\mu \Phi - \frac{i}{2} g \left(\vec{\tau} \cdot \vec{W}_L \Phi - \Phi \vec{\tau} \cdot \vec{W}_R \right),\end{aligned}$$

generates the gauge boson mass matrices after SSB.

Defining $W_{L,R\mu}^\pm \equiv (W_{L,R\mu}^1 \mp iW_{L,R\mu}^2)/\sqrt{2}$, the charged gauge boson mass matrix in the basis (W_L^\pm, W_R^\pm) with $k_2 = 0$ is block diagonal,

$$M_{W^\pm}^2 = \frac{g^2}{4} \begin{pmatrix} k_1^2 & 0 \\ 0 & k_1^2 + v_R^2 \end{pmatrix}.\tag{21}$$

The absence of off-diagonal entries follows directly from $k_2 = 0$ (the off-diagonal element $\propto k_1 k_2$), so W and W' do not mix in our approximation. The physical masses are

$$m_W^2 \approx \frac{g^2 k_1^2}{4}, \quad m_{W'}^2 \approx \frac{g^2 v_R^2}{4}.$$

In the basis $(W_{\mu L}^3, W_{\mu R}^3, B_\mu)$, the neutral gauge boson mass matrix is

$$M_Z^2 = \frac{1}{4} \begin{pmatrix} g^2 k_1^2 & -g^2 k_1^2 & 0 \\ -g^2 k_1^2 & g^2 (k_1^2 + v_R^2) & -gg_{B-L} v_R^2 \\ 0 & -gg_{B-L} v_R^2 & g_{B-L}^2 v_R^2 \end{pmatrix} \quad (22)$$

which is diagonalized in two steps (see Appendix A). In the limit $k_1 \ll v_R$ the $Z - Z'$ mixing angle satisfies $\zeta \approx 0$, and the gauge eigenstates are expressed in terms of the mass eigenstates (A_μ, Z_μ, Z'_μ) as

$$\begin{aligned} W_{\mu L}^3 &= A_\mu \sin \theta_W - Z_\mu \cos \theta_W, \\ W_{\mu R}^3 &= A_\mu \sin \theta_W + Z_\mu \sin \theta_W \tan \theta_W - Z'_\mu \frac{\sqrt{\cos(2\theta_W)}}{\cos \theta_W}, \\ B_\mu &= A_\mu \sqrt{\cos(2\theta_W)} + Z_\mu \sqrt{\cos(2\theta_W)} \tan \theta_W + Z'_\mu \tan \theta_W. \end{aligned} \quad (23)$$

The physical neutral gauge boson masses in this limit are

$$m_Z^2 = \frac{m_W^2}{\cos^2 \theta_W}, \quad m_{Z'}^2 = m_W^2 \frac{\cos^2 \theta_W}{\cos(2\theta_W)} - m_W^2 \frac{(\tan(2\theta_W) + 4) \tan^2 \theta_W}{4}.$$

From the covariant derivatives and the field rotation (23), the interactions of charged leptons with the neutral gauge bosons are

$$\begin{aligned} \mathcal{L}_{Z\ell\ell} &= \frac{ig}{4 \cos \theta_W} Z \bar{\ell} \gamma^\mu [(3 \sin^2 \theta_W - \cos^2 \theta_W) + \gamma^5] \ell, \\ \mathcal{L}_{Z'\ell\ell} &= \frac{ig}{4 \cos \theta_W \sqrt{\cos(2\theta_W)}} Z' \bar{\ell} \gamma^\mu [(2 \sin^2 \theta_W - \cos(2\theta_W)) - \cos(2\theta_W) \gamma^5] \ell. \end{aligned} \quad (24)$$

3 The inverse seesaw

The DLRSM naturally accommodates the inverse seesaw (ISS) mechanism as an alternative to the standard seesaw. Whereas in type-I seesaw the right handed neutrino mass $M_R \sim 10^{14}$ GeV is inaccessibly large, the ISS achieves the observed light neutrino mass scale via a small lepton-number-breaking parameter μ_S , keeping $M_D \propto v_R$ at the TeV scale where it can be probed at colliders.

3.1 Yukawa Lagrangian and mass matrices

The lepton Yukawa Lagrangian, invariant under G_{LR} and the parity symmetry, is [19, 20]

$$-\mathcal{L}_Y = \bar{L}_L Y \Phi L_R + \bar{L}_L \tilde{Y} \tilde{\Phi} L_R + \bar{S} Y_L \tilde{\chi}_L^\dagger L_L + \bar{S}^c Y_R \tilde{\chi}_R^\dagger L_R + \frac{1}{2} \bar{S}^c \mu_S S + \text{h.c.}, \quad (25)$$

where Y, \tilde{Y}, Y_L, Y_R are 3×3 complex Yukawa matrices, μ_S is the Majorana mass matrix for fermionic singlets S_i , and we use $\tilde{X} \equiv i\sigma_2 X^*$ for scalar doublets and $S^c = C \bar{S}^\top$ for the charge conjugate of S .

The parity symmetry, combining (5) and (9), imposes

$$Y_L = Y_R, \quad Y = Y^\dagger, \quad \tilde{Y} = \tilde{Y}^\dagger, \quad \mu_S = \mu_S^\dagger, \quad (26)$$

above the LR symmetry breaking scale. After SSB the lepton mass matrices read

$$M_\ell = \frac{k_1}{\sqrt{2}} \tilde{Y}, \quad m_D = \frac{k_1}{\sqrt{2}} Y, \quad M_D = \frac{v_R}{\sqrt{2}} Y_R. \quad (27)$$

where M_ℓ is the charged-lepton mass matrix, m_D is the light-heavy Dirac neutrino mass matrix, and M_D is the heavy Majorana mass matrix for the right-handed neutrinos. The charged lepton masses are extracted via a biunitary transformation,

$$\hat{M}_\ell = V_L^{\ell\dagger} M_\ell V_R^\ell = \text{diag}(m_e, m_\mu, m_\tau). \quad (28)$$

3.2 Neutrino mass matrix and spectrum

In the basis $n'_L = (\nu_L, \nu_R^c, S^c)$, $n'_R = (\nu_L^c, \nu_R, S)$ the full 9×9 neutrino Majorana mass matrix takes the ISS block form

$$\mathcal{M}_\nu = \begin{pmatrix} 0 & B^\top \\ B & C \end{pmatrix}, \quad B = \begin{pmatrix} m_D \\ 0 \end{pmatrix}, \quad C = \begin{pmatrix} 0 & M_D^\top \\ M_D & \mu_S \end{pmatrix}. \quad (29)$$

In the hierarchy $|C| \gg |B|$, the seesaw formula gives the light neutrino mass matrix

$$m_\nu \approx m_D^\top M_D^{-1} \mu_S (M_D^\top)^{-1} m_D. \quad (30)$$

Note that $m_\nu \propto \mu_S$: in contrast to the type-I seesaw, the light-neutrino masses can be small even for $M_D \sim v_R \sim \mathcal{O}(\text{TeV})$, provided $\mu_S \ll m_D$. The heavy states form pseudo-Dirac pairs N_i^\pm with degenerate masses

$$M_i^- \approx M_i^+ \approx M_{Di}, \quad (31)$$

split at $\mathcal{O}(\mu_S)$.

3.3 Mixing matrix and Casas-Ibarra parametrization

Defining the active-sterile mixing parameter

$$\xi \equiv m_D^\top M_D^{-1} \quad (32)$$

and imposing $M_D^{-1} \mu_S M_D^{-1} m_D \approx 0$, the approximate mixing matrix is [21, 22]

$$\mathcal{U} \approx \begin{pmatrix} U_\nu & -\frac{i}{\sqrt{2}}\xi & \frac{1}{\sqrt{2}}\xi \\ 0 & \frac{i}{\sqrt{2}}\mathbb{I} & \frac{1}{\sqrt{2}}\mathbb{I} \\ -\xi^\top U_\nu & -\frac{i}{\sqrt{2}}\mathbb{I} & \frac{1}{\sqrt{2}}\mathbb{I} \end{pmatrix} \quad (33)$$

where U_ν is the unitary matrix that diagonalizes the light neutrino mass matrix (30).

The 9×9 PMNS-like matrix \mathcal{U} diagonalizes \mathcal{M}_ν and can be decomposed into three 3×9 block matrices,

$$\mathcal{U} = \begin{pmatrix} U_L \\ U_R \\ U_S \end{pmatrix},$$

such that

$$\hat{\mathcal{M}}_\nu = \mathcal{U}^\top \mathcal{M}_\nu \mathcal{U} = \text{diag}(m_i, M_i^-, M_i^+).$$

The unitary condition $U_X U_Y^\dagger = \delta_{XY} \mathbb{I}$ ($X, Y = L, R, S$) yields the identities

$$m_D = U_R^* \hat{\mathcal{M}}_\nu U_L^\dagger, \quad M_D = U_S^* \hat{\mathcal{M}}_\nu U_R^\dagger, \quad \mu_S = U_S^* \hat{\mathcal{M}}_\nu U_S^\dagger. \quad (34)$$

The light-neutrino (30) can be rewritten as

$$m_\nu \approx m_D^\top \mathcal{M}^{-1} m_D; \quad \mathcal{M} = M_D \mu_S^{-1} M_D^\top. \quad (35)$$

and by means of the Casas-Ibarra parametrization the Dirac neutrino mass matrix is written as follows [23, 24]

$$m_D = V^\dagger \text{diag}(\sqrt{\mathcal{M}_1}, \sqrt{\mathcal{M}_2}, \sqrt{\mathcal{M}_3}) R \text{diag}(\sqrt{m_{\nu_1}}, \sqrt{m_{\nu_2}}, \sqrt{m_{\nu_3}}) U_\nu^\dagger, \quad (36)$$

where V diagonalises \mathcal{M} and R is a complex orthogonal matrix ($RR^\top = \mathbb{I}$) that parametrises the remaining freedom in m_D consistent with the light neutrino spectrum. In the simplified diagonal ansatz used in the numerical analysis, $M_D = \text{diag}(M_{D1}, M_{D2}, M_{D3})$, $\mu_S = \text{diag}(\mu_{S1}, \mu_{S2}, \mu_{S3})$, $R = \mathbb{I}$, then, $V = \mathbb{I}$ and

$$m_D = \text{diag}\left(\sqrt{\frac{m_{\nu_1}}{\mu_{S1}}} M_{D1}, \sqrt{\frac{m_{\nu_2}}{\mu_{S2}}} M_{D2}, \sqrt{\frac{m_{\nu_3}}{\mu_{S3}}} M_{D3}\right) U_\nu^\dagger \quad (37)$$

3.4 Neutrino mass basis and charged currents

The weak neutrino states are rotated to the mass eigenstates $n = (\nu_i, N_i^-, N_i^+)$ by

$$n'_L = \mathcal{U}^* n_L, \quad n'_R = \mathcal{U} n_R.$$

The charged-current Lagrangian mediated by W, W' is

$$\mathcal{L}_W = \frac{g}{2} W^+ \bar{n}_i \gamma^\mu P_L Q_{L,ai}^* \ell_a + \frac{g}{2} W'^+ \bar{n}_i \gamma^\mu P_R Q_{R,ai}^* \ell_a + \text{h.c.}, \quad (38)$$

where the left and right leptonic mixing matrices are

$$Q_L = V_L^{\ell\dagger} U_L^*, \quad Q_R = V_R^{\ell\dagger} U_R. \quad (39)$$

3.5 Yukawa interactions

In the unitary gauge the Goldstone bosons are absent; retaining only physical scalars (see Section 2.2) the Yukawa Lagrangian (25) decomposes into neutral and charged parts.

The interactions of neutral Higgs bosons with charged leptons read

$$-\mathcal{L}_Y^0 \supset \frac{m_\ell}{k_1} h^{SM} \bar{\ell} \ell + \frac{m_\ell \alpha_{13}}{2\rho_1 v_R} H_2^0 \bar{\ell} \ell + \left(\frac{1}{k_1} H_3^0 \bar{\ell} \Lambda P_R \ell + \frac{i}{k_1} A_1^0 \bar{\ell} \Lambda P_R \ell + \text{h.c.} \right) \quad (40)$$

where

$$\Lambda = V_L^{\ell\dagger} m_D V_R^\ell. \quad (41)$$

The matrix Λ in (41) is the combination of m_D and the charged leptonic diagonalisation matrices that controls the flavour-changing couplings of H_3^0 and A_1^0 to charged leptons. Note that both H_3^0 and A_1^0 enter through the same combination ΛP_R ; the only difference between their couplings is the factor of i for A_1^0 in (40), which is a pure phase and does not affect $|\Lambda|^2$ in the squared amplitude, the reason both contribute to a_μ with the same parametric dependence (see Section 4.1).

The charged scalars interactions with leptons and neutrinos are

$$-\mathcal{L}_Y^\pm = \frac{1}{\sqrt{2}} H_R^\pm \bar{n} \left(\left(K - \frac{k_1}{v_R} D \right) P_R - \tilde{T} P_L \right) \ell - \frac{1}{\sqrt{2}} H_L^\pm \bar{n} E P_L \ell + \text{h.c.} \quad (42)$$

with the mixing matrices defined as

$$\begin{aligned} K &= U_L^\top Y V_R^\ell & D &= U_S^\top Y_R V_R^\ell \\ \tilde{T} &= U_R^\dagger \tilde{Y}^\dagger V_L^\ell & E &= U_S^\dagger Y_L V_L^\ell \end{aligned} \quad (43)$$

4 One loop contributions to $(g - 2)_\mu$

Within the DLRSM, supplemented by the inverse seesaw, the anomalous magnetic moment of the muon receives one-loop corrections from five classes of new particles: the neutral gauge boson Z' , the charged gauge boson W' , the heavy charged scalars $H_{L,R}^\pm$ and the neutral scalars $H_{2,3}^0, A_1^0$. Table 2 lists the diagram topologies and their internal particle content. Throughout this section we work in the unitary gauge, set $V_L^\ell = V_R^\ell = \mathbb{1}$ for simplicity, and use the general formulae for a_μ new physics contributions from [25] and summarized in Appendix B. The Feynman diagrams are shown in Figs. 1 and 2. Finally the total contribution to a_μ is given by

$$\Delta a_\mu^{\text{DLRSM}} = \sum_{\Theta} a_\mu(\Theta). \quad (44)$$

Θ	P_0	P_1	P_2	Θ	P_0	P_1	P_2
FVV	n_i	W'	W'	VFF	Z'	μ	μ
FSS	n_i	H_R^\pm	H_R^\mp	SFF	H_i^0	ℓ	ℓ
FSS	n_i	H_L^\pm	H_L^\mp	SFF	A_1^0	ℓ	ℓ

Table 2: One loop diagram topologies contributing to a_μ in the DLRSM. The notation $\Theta(P_0, P_1, P_2)$ identifies the topology and the particles in the loop: P_0 is the internal neutral fermion (F) or boson (B) connecting to the external muon lines, while P_1 and P_2 are the two internal propagators closing the loop.

4.1 Neutral contributions SFF and VFF topologies

For the neutral scalars, a_μ has contributions of the left Feynman diagram in Figure 1, we consider the approximation $m_\ell \ll M_S$ ($\lambda \rightarrow 0$) with $S = H_{2,3}^0, A_1^0$. From (40), the couplings of $H_{2,3}^0$ and A_1^0 with contributions to a_μ are, respectively

$$H_2^0 : C_S = \frac{m_\mu \alpha_{13}}{2\rho_1 v_R}, \quad C_P = 0; \quad (45)$$

$$H_3^0 : C_S = -\frac{1}{\sqrt{2}} Y_{\ell\mu}, \quad C_P = 0; \quad (46)$$

$$A_1^0 : C_S = 0, \quad C_P = -\frac{i}{\sqrt{2}} Y_{\ell\mu}, \quad (47)$$

for Y real (27), so that,

$$\begin{aligned} a_\mu(H_2^0 \mu\mu) &\approx \frac{m_\mu^2}{16\pi^2 M_{H_2^0}^2} \left(\frac{m_\mu \alpha_{13}}{2\rho_1 v_R} \right)^2 \left(4 \log \left(\frac{m_\mu}{M_{H_2^0}} \right) + 3 \right), \\ a_\mu(H_3^0 \ell\ell) &\approx \frac{1}{32\pi^2} \frac{m_\mu}{M_{H_3^0}^2} \sum_\ell m_\ell |Y_{\ell\mu}|^2 \left(4 \log \left(\frac{m_\ell}{M_{H_3^0}} \right) + 3 \right), \\ a_\mu(A_1^0 \ell\ell) &\approx -\frac{1}{32\pi^2} \frac{m_\mu}{M_{A_1^0}^2} \sum_\ell m_\ell |Y_{\ell\mu}|^2 \left(4 \log \left(\frac{m_\ell}{M_{A_1^0}} \right) + 3 \right). \end{aligned} \quad (48)$$

The contributions of neutral scalars $S = H_{2,3}^0, A_1^0$ are proportional to $\left(\frac{m_\mu}{M_S}\right)^2$, but in particular the H_2^0 contribution is suppressed additionally by the coupling of interaction $H_2^0 \mu\mu$ which give a factor proportional to $\left(\frac{m_\mu}{v_R}\right)^2$, in consequence $a_\mu(H_2^0)$ is negligible for large v_R . The contributions to a_μ from H_3^0 and A_1^0 are of equal magnitude in the case of $\delta^0 = 0$, from (20) where the two masses are degenerated and cancel each other. In the case of $\delta^0 \neq 0$, the values of λ_{2356} and λ_{2456} contributes negligibly at the limit $k_1 \ll v_R$. Focusing on H_3^0 contribution we observe that $\log\left(\frac{m_\ell}{M_{H_3^0}}\right)$ is expected to be negative for large values of $M_{H_3^0}$ which is proportional to v_R , in consequence, $a_\mu(H_3^0 \ell\ell) < 0$, the same argument applies to H_2^0 contribution, and for A_1^0 this implies $a_\mu(A_1^0 \ell\ell) > 0$.

For a neutral vector boson V , a_μ has contributions from Feynman diagram in the right Figure 1. Reading off C_V and C_A from the interaction Lagrangian (24) and substituting in (66) in the approximation $m_\ell \ll M_{Z'}$,

$$a_\mu(Z' \mu\mu) \approx -\frac{1}{12\pi^2} \frac{g^2}{16 \cos^2 \theta_W \cos(2\theta_W)} \left(\frac{m_\mu}{M_{Z'}} \right)^2 \left(5 \cos^2(2\theta_W) - (2 \sin^2 \theta_W - \cos(2\theta_W))^2 \right).$$

With $\sin^2 \theta_W \approx 0.231$ the bracket evaluates to approximately 1.5, so $a_\mu(Z') < 0$.

4.2 Charged contributions: SFF and FVV topologies

The FSS diagram have neutrinos in the loop and charged scalars $H_{L,R}^\pm$ as the two internal propagators (left Feynman diagram in Figure 2). We treat the two neutrino mass scales separately: light neutrinos ($m_n \approx 0, m_\mu \ll M_S$) and heavy neutrinos $M_F = m_n, (m_\mu \ll M_S, m_n)$. The general FSS formula in each limit is

$$a_\mu(n, S^\pm) \approx \begin{cases} -\frac{1}{48\pi^2} \left(\frac{m_\mu}{M_{S^\pm}} \right)^2 (|C_P|^2 + |C_S|^2) & m_n \approx 0, m_\mu \ll M_S, \\ \frac{1}{16\pi^2} \sum_{n=4}^9 \left(\frac{m_\mu}{m_n} \right) (|C_P|^2 - |C_S|^2) \mathcal{G}\left(\frac{M_{S^\pm}}{m_n}\right) & m_\mu \ll M_S, m_n. \end{cases} \quad (49)$$

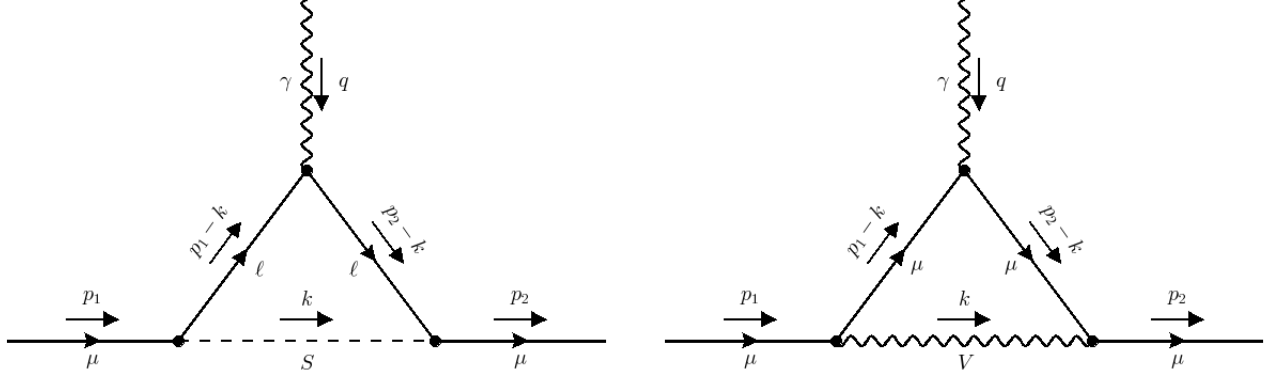


Figure 1: Feynman diagrams for neutral exchange bosons SFF (left) and VFF (right) topologies

where

$$\mathcal{G}(r) = \frac{1 - 4r^2 \log r - r^4}{(1 - r^2)^3}. \quad (50)$$

Substituting the couplings from (42) in (49) gives the explicit $H_{L,R}^\pm$ contributions:

$$\begin{aligned} a_\mu(n, H_L^\pm) &\approx 0, \\ a_\mu(n, H_R^\pm) &\approx \frac{1}{16\pi^2} \frac{1}{4} \sum_{n=4}^9 \left(\frac{m_\mu}{m_n}\right) \mathcal{G}\left(\frac{M_{H_R^\pm}}{m_n}\right) \text{Re}\left(K_{n\mu} \tilde{T}_{n\mu}^*\right), \end{aligned}$$

neglecting light neutrino contributions. From (42), the interaction of H_L^\pm with leptons is purely chiral in consequence $|C_P(H_L^\pm)|^2 - |C_S(H_L^\pm)|^2 = 0$. The contribution $a_\mu(n, H_R^\pm)$ depends on $M_{H_R^\pm}/m_n$, encoding the mass dependence on α_{23} .

For the FVV topology for charged gauge boson (right feynman diagram in Figure 2) the a_μ contribution is given by

$$a_\mu(FVV) \approx \begin{cases} \frac{5}{24\pi^2} \left(\frac{m_\mu}{M_V}\right)^2 (|C_V|^2 + |C_A|^2) & m_F \approx 0, m_\mu \ll M_V, \\ \frac{1}{16\pi^2} \left[\left(\frac{m_\mu}{m_n}\right)^2 \mathcal{F}_+ \left(\frac{M_V}{m_n}\right) (|C_V|^2 + |C_A|^2) - \left(\frac{m_\mu}{m_n}\right) \mathcal{F}_- \left(\frac{M_V}{m_n}\right) (|C_V|^2 - |C_A|^2) \right] & m_\mu \ll M_F, M_V \end{cases} \quad (51)$$

where

$$\begin{aligned} \mathcal{F}_+(r) &= \frac{1}{3r^2(1-r^2)^3} [4 + 35r^2 - 43r^4 + 10r^6], \\ \mathcal{F}_-(r) &= \frac{1}{r^2(1-r^2)^3} [1 + 12r^2 + 20r^2 \log r - 17r^4 + 4r^6], \end{aligned}$$

For the W' loop the coupling to $n_i\mu$ is purely chiral (38), so $C_V = C_A = gQ_{R,n\mu}/2$. Substituting from (51),

$$a_\mu(nW'W') \approx \frac{1}{8\pi^2} \frac{g^2}{4} \left[\frac{5}{3} \left(\frac{m_\mu}{M_{W'}}\right)^2 \sum_{n=1}^3 |Q_{R,n\mu}|^2 + \frac{1}{2} \left(\frac{m_\mu}{m_n}\right)^2 \sum_{n=4}^9 |Q_{R,n\mu}|^2 \mathcal{F}_+ \left(\frac{M_{W'}}{m_n}\right) \right]. \quad (52)$$

Finally, Table 3 collects the parametric scaling of each contribution

5 Numerical Analysis

The light neutrino mixing angles and mass-squared differences are fixed to the Normal Ordering (NO) best fit values from the NuFit collaboration [26], summarized in Table 4. These enter the analysis through the Casas-Ibarra parametrization (37), which expresses m_D in terms of M_D , μ_X and neutrino masses m_n .

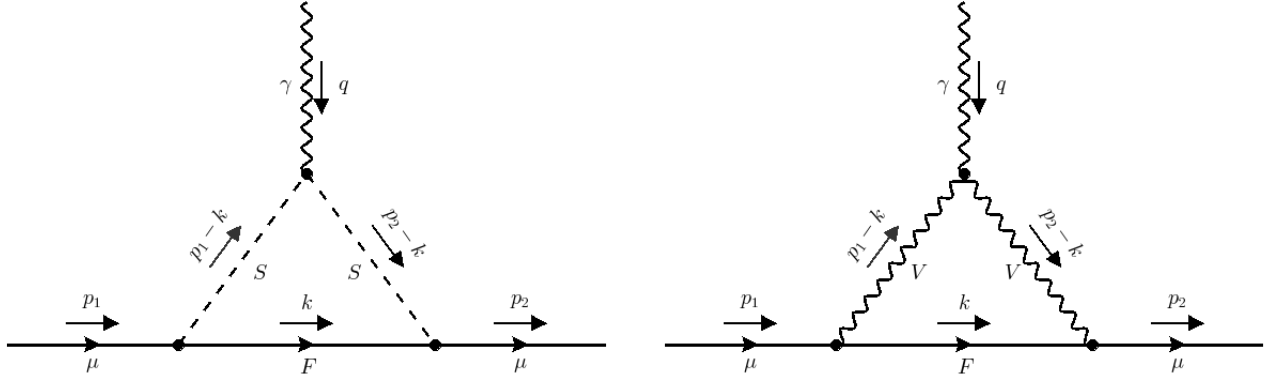


Figure 2: Feynman diagrams for the FSS (left) and FVV (right) topologies

Contribution	Scaling	Sign
$a_\mu(Z')$	g^2/v_R^2	-
$a_\mu(W')$	g^2/v_R^2	+
$a_\mu(H_3^0)$	$Y_R^2/(\alpha_{23}v_R^2)$	-
$a_\mu(A_1^0)$	$Y_R^2/(\alpha_{23}v_R^2)$	+
$a_\mu(H_R^\pm)$	$Y_R^2/(\alpha_{23}v_R^4)$	mixed
$a_\mu(H_L^\pm)$	Y_L^2/v_R^4	0
$a_\mu(H_2^0)$	$\alpha_{13}^2 m_\mu^2/v_R^4$	-

Table 3: Leading parametric scaling of each one-loop contribution to a_μ with the DLRSB parameters.

	Normal Ordering (best fit)	
	bf $\pm 1\sigma$	3σ range
$\sin^2 \theta_{12}$	$0.308_{-0.011}^{+0.012}$	$0.275 \rightarrow 0.345$
$\sin^2 \theta_{23}$	$0.470_{-0.013}^{+0.017}$	$0.435 \rightarrow 0.585$
$\sin^2 \theta_{13}$	$0.02215_{-0.00058}^{+0.00056}$	$0.02030 \rightarrow 0.02388$
$\delta_{\text{CP}}/^\circ$	212_{-41}^{+26}	$124 \rightarrow 364$
$\Delta m_{21}^2/10^{-5} \text{eV}^2$	$7.49_{-0.19}^{+0.19}$	$6.92 \rightarrow 8.05$
$\Delta m_{31}^2/10^{-3} \text{eV}^2$	$+2.513_{-0.019}^{+0.021}$	$+2.451 \rightarrow +2.578$

Table 4: Normal ordering best-fit values and 3σ ranges for neutrino oscillation parameters, taken from NuFit global analysis [26].

We set $\lambda_{12} = \rho_1 = 1$, which fixes the SM-like Higgs mass condition from Table 1 to

$$\alpha_{13}^2 \approx 2 \left(2 - \frac{m_{H_1^0}^2}{k_1^2} \right) \approx 1.87, \quad M_{H_2^0}^2 \approx 2 \left(v_R^2 + 2k_1^2 - m_{H_1^0}^2 \right) \approx 2v_R^2.$$

The masses H_3^0 , A_1^0 , H_R^\pm are then controlled by α_{23} alone (at leading order in v_R , see Table 1). Requiring $M_{H_3^0} > M_{H_1^0}$ sets a lower bound

$$\alpha_{23} > 2 \frac{M_{H_1^0}^2}{v_R^2}. \quad (53)$$

which over the range $v_R \in [10^3, 10^6]$ GeV, implies $\alpha_{23}^{\min} \in [10^{-8}, 10^{-2}]$.

For simplicity, we take the degenerate limit

$$M_i^- \approx M_i^+ = M = \frac{Y_R}{\sqrt{2}} v_R, \quad \mu_{S1} = \mu_{S2} = \mu_{S3} \equiv \mu_X, \quad (54)$$

which reduces the heavy neutrino space. In this limit, we could approximate

$$Y_{ij} \approx \frac{\sqrt{m_{\text{light}}}}{\sqrt{\mu_X}} \frac{v_R}{k_1} \mathcal{O}(0.1) \quad (55)$$

where we fix the elements of U_ν to be of order $\mathcal{O}(0.1)$ and $Y_R \sim 1$, but the Yukawa couplings are constrained by perturbativity $|Y_{ij}|^2 < 6\pi$, consequently, from (55)

$$\left(\frac{\text{GeV}}{\mu_X} \right) \left(\frac{v_R^2}{\text{GeV}^2} \right) \lesssim 10^{19}, \quad (56)$$

assuming a light-neutrino mass scale of order $\mathcal{O}(10^{-12})$ GeV. The free parameters of the analysis are therefore v_R , Y_R , μ_X and α_{23} .

5.1 Dependence on individual parameters

In Figures 3 and 4 we vary Y_R and v_R parameter individually, respectively, while fixing the remaining three to the reference values

$$Y_R = 0.1, \quad \alpha_{23} = 10^{-6}, \quad \mu_X = 1 \text{ MeV}, \quad v_R = 10 \text{ TeV}. \quad (57)$$

On Figure 3, the behavior of a_μ as a function of Y_R is shown. We observe that the most important contribution to a_μ comes from W' in the left panel of Figure 3, the remaining contributions are negligible in comparison. The total value of $\Delta a_\mu^{\text{DLRSM}}$ at low values of Y_R requires $Y_R \gtrsim 10^{-1}$ to satisfy the experimental 1σ band.

Similarly, in left panel of Figure 4, the individual contributions to a_μ are shown and we observe a similar behavior to the case of Y_R . In this case, the W' contributions is the most relevant contribution. The total $\Delta a_\mu^{\text{DLRSM}}$ is constrained to values of $v_R \gtrsim 1$ TeV.

To assess the robustness of the proposed solution across the full multi-dimensional parameter space, we performed a random scan varying the symmetry breaking scale v_R , the heavy neutrino Yukawa coupling Y_R , the inverse seesaw parameter μ_X , and the scalar potential parameter α_{23} simultaneously, the range of the scan are as follows

$$v_R \in [500, 10^4] \text{ GeV}, \quad Y_R \in [10^{-1}, 1], \quad \mu_X \in [10^{-6}, 1] \text{ GeV}, \quad \alpha_{23} \in [10^{-8}, 10^{-4}]. \quad (58)$$

The resulting viability regions are projected onto the (v_R, μ_X) , (v_R, Y_R) , and (v_R, α_{23}) planes in Figure 5. A striking feature across all distributions is the sharp boundary at $v_R \lesssim 1$ TeV, below which the model generally overpredicts the anomalous magnetic moment, resulting in contributions exceeding the 2σ experimental upper bound (indicated by gray points). Above this threshold, particularly for $v_R \gtrsim 1$ TeV, we observe a dense population of viable points (green) that satisfy the 1σ constraint. This viable window is remarkably insensitive to variations in μ_X and α_{23} over several orders of magnitude, confirming that the W' boson mass acts as the primary control parameter. The projection onto the (v_R, Y_R) plane further shows that reducing Y_R below ~ 0.1 leads to an underprediction of $\Delta a_\mu^{\text{DLRSM}}$, incompatible with the 1σ experimental band

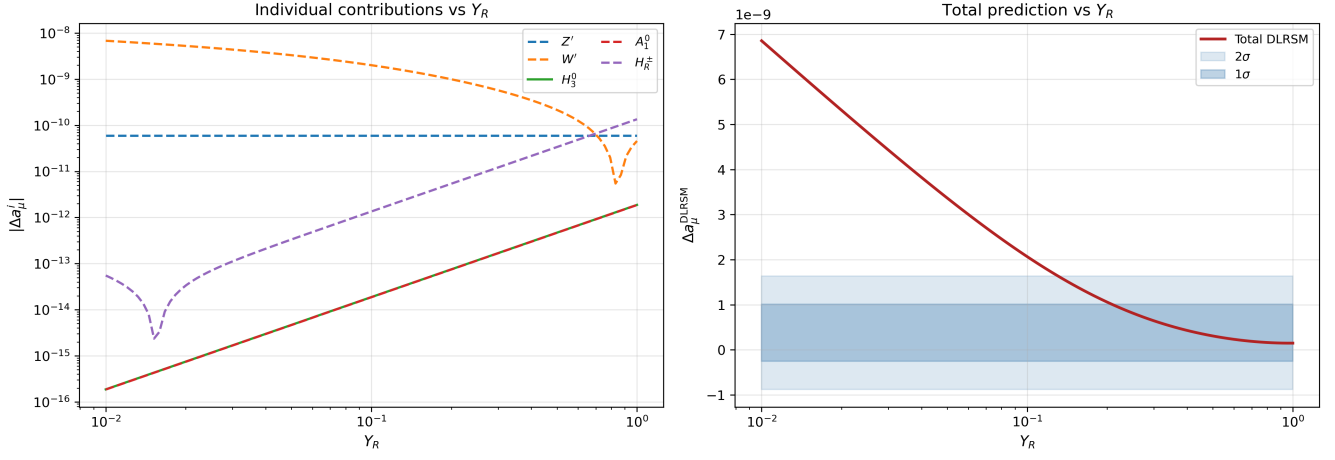


Figure 3: Dependence of Δa_μ on the Yukawa coupling Y_R , with $v_R = 10$ TeV, $\alpha_{23} = 10^{-6}$, $\mu_X = 1$ MeV. Left: Individual contributions $|\Delta a_\mu^i|$. Right: Total prediction $\Delta a_\mu^{\text{DLRSM}}$ with experimental bands.

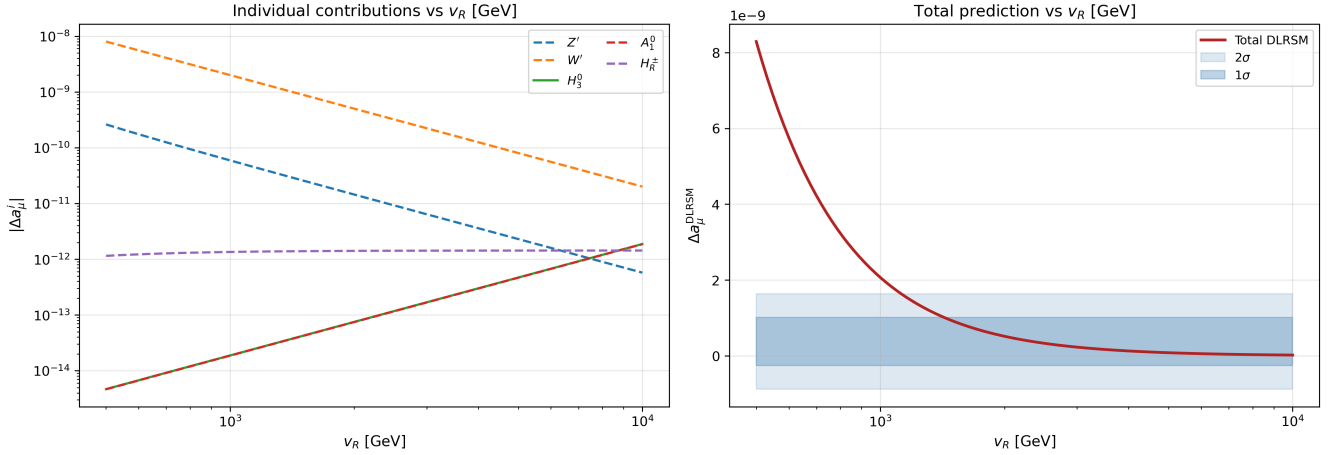


Figure 4: Dependence of Δa_μ on the symmetry breaking scale v_R , with $Y_R = 0.1$, $\alpha_{23} = 10^{-6}$, $\mu_X = 1$ MeV. Left: Individual contributions $|\Delta a_\mu^i|$. Right: Total prediction $\Delta a_\mu^{\text{DLRSM}}$ compared to experimental bands.

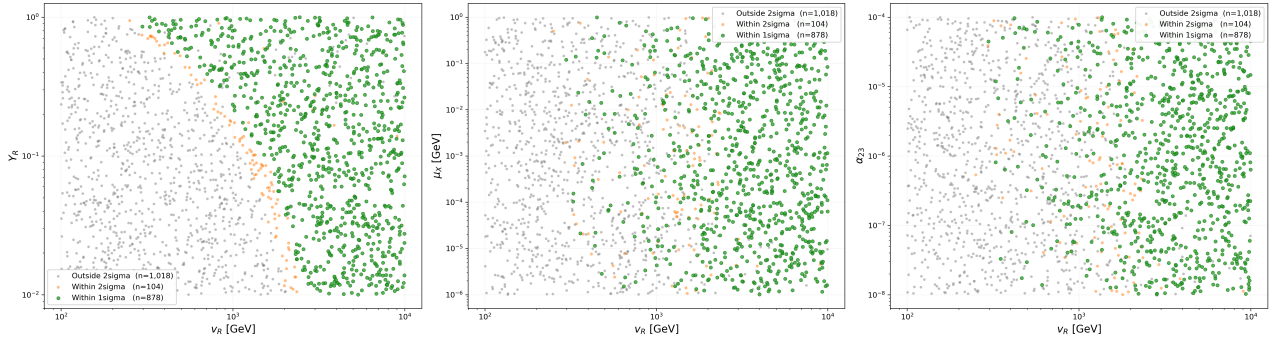


Figure 5: Results of a multi-parameter random scan projected onto the planes of (v_R, Y_R) (left), (v_R, μ_X) (center), and (v_R, α_{23}) (right). Points are color-coded based on their consistency with the experimental measurement of Δa_μ : green points lie within the 1σ band, orange points within the 2σ band, and gray points fall outside the 2σ allowed region. The clear stratification demonstrates that the viability of the DLRSM solution is primarily determined by the symmetry breaking scale v_R , favoring a window starting at approximately 1 TeV, largely independent of the specific values of the other model parameters.

The analysis points toward new gauge boson masses $m_{W'} \gtrsim 325$ GeV, $m_{Z'} \gtrsim 385$ GeV in the MLRS condition and heavy neutrinos $m_n \gtrsim 700$ GeV. If we consider $g_R \neq g_L$, the masses of new gauge bosons are as follows

$$M_{W'}^2 \approx \frac{1}{4} g_R^2 v_R^2, \quad M_{Z'}^2 \approx \frac{v_R^2}{4} (g_R^2 + g_{BL}^2). \quad (59)$$

In this case, the $a_\mu(W')$ it is not sensitive to the values of g_R as a consequence of the scaling of this contribution

$$a_\mu(W') \propto \frac{g_R^2}{m_{W'}^2} \approx \frac{1}{v_R^2}, \quad (60)$$

and we can conclude similarly that $v_R \gtrsim 1$ TeV, if we consider the perturbative limit

$$\frac{g_R^2}{4\pi} \lesssim 1, \quad (61)$$

this points toward new gauge boson masses $m_{W'} \gtrsim 1625$ GeV, $m_{Z'} \gtrsim 1650$ GeV for $g_R = 5g_L$, near to the perturbative limit (61).

6 Conclusions

The experimental result for Δa_μ , now consistent with the Standard Model prediction within uncertainties, allows us to place meaningful bounds on the parameter space of the DLRSM rather than interpret the discrepancy as a signal of new physics. The dominant new-physics contributions arise from the extended neutral and charged gauge sectors, specifically from Z' and W' loops, while contributions from the new scalar sector are generally subdominant except at small values of α_{23} , where the charged scalar H_R^\pm become relevant. The parameter μ_X , which controls the small Majorana mass splitting in the inverse seesaw, is found to have negligible impact on $\Delta a_\mu^{\text{DLRSM}}$, reflecting the decoupling of the lightest neutrino mass scale from the observables sensitive to the heavier spectrum. Our scan over the free parameters establishes that $v_R \lesssim 1$ TeV is excluded by the $g - 2$ constraint at the benchmark values considered, consequently, the analysis points toward new gauge boson masses $m_{W'} \gtrsim 325$ GeV, $m_{Z'} \gtrsim 385$ GeV in the MLRS condition and heavy neutrinos $m_n \gtrsim 700$ GeV. In the case of $g_R \neq g_L$, the lower bounds could be stronger such as $m_{W'} \gtrsim 1625$ GeV, $m_{Z'} \gtrsim 1650$ GeV.

Acknowledgments

The research presented herein has been supported by the UNAM Postdoctoral Program (POSDOC) and the PAPIIT project IN105825.

A Neutral gauge boson matrix diagonalization

The neutral gauge boson mass matrix M_Z^2 in (22) can be reduced to a block diagonal matrix by

$$R = \begin{pmatrix} \sin \theta_W & -\cos \theta_W & 0 \\ \sin \theta_W & \sin \theta_W \tan \theta_W & -\frac{\sqrt{\cos(2\theta_W)}}{\cos \theta_W} \\ \sqrt{\cos(2\theta_W)} & \sqrt{\cos(2\theta_W)} \tan \theta_W & \tan \theta_W \end{pmatrix} \quad (62)$$

with the following definitions

$$\begin{aligned} e &= g \sin \theta_W, \\ \frac{1}{e^2} &= \frac{2}{g^2} + \frac{1}{g_{B-L}^2}, \end{aligned} \quad (63)$$

Then, the obtained block diagonal matrix

$$\begin{aligned} M_0^2 &= R^\top M_Z^2 R \\ &= \begin{pmatrix} 0 & 0 & 0 \\ 0 & \frac{g^2(k_1^2+k_2^2)}{4\cos^2\theta_W} & -\frac{gg_{B-L}(k_1^2+k_2^2)}{2\cos\theta_W\tan(2\theta_W)} \\ 0 & -\frac{gg_{B-L}(k_1^2+k_2^2)}{2\cos\theta_W\tan(2\theta_W)} & \frac{g^2v_R^2\cos^2\theta_W}{4\cos(2\theta_W)} + \frac{g^2(k_1^2+k_2^2)\cos(2\theta_W)}{4\cos^2\theta_W} \end{pmatrix} \end{aligned}$$

which can be diagonalized by the rotation matrix $O(\zeta)$ over the angle ζ given by

$$\begin{aligned} O(\zeta) &= \begin{pmatrix} 1 & 0 & 0 \\ 0 & \cos(\zeta) & \sin(\zeta) \\ 0 & -\sin(\zeta) & \cos(\zeta) \end{pmatrix}, \\ \tan|2\zeta| &\approx \frac{4g_{B-L}(k_1^2+k_2^2)\cos(2\theta_W)}{gv_R^2\cos^3\theta_W\tan(2\theta_W)}. \end{aligned} \quad (64)$$

In addition, with $R_Z = O(\zeta)R$ the neutral gauge boson matrix (22), is diagonalized by

$$\hat{M}_Z^2 = R_Z^\top M_Z^2 R_Z. \quad (65)$$

B Master formulas for the one-loop contributions to $(g-2)_\mu$

This appendix collects the master integrals for one loop contributions to $a_\mu = (g-2)_\mu/2$ following the notation of [25].

B.1 General structure and notation

The generic one-loop correction to a_μ from a diagram with internal boson mass M_B , internal fermions mass m_F , couplings coefficients C_X , takes the form

$$a_\mu = \frac{m_\mu^2}{8\pi^2 M_B^2} \sum_X |C_X|^2 \mathcal{L}_X(\epsilon, \lambda), \quad (66)$$

where the dimensionless parameters are

$$\epsilon = \frac{m_F}{m_\mu}, \quad \lambda = \frac{m_\mu}{M_B}.$$

The index X runs over the distinct coupling structures entering the diagram $X = S, P, V, A$ and the loop function is given by

$$\mathcal{L}_X(\epsilon, \lambda) = \int_0^1 \frac{Q_X(x, \epsilon, \lambda)}{\mathcal{D}(x, \epsilon, \lambda)} dx. \quad (67)$$

Θ	Figure	Numerator	Denominator
VFF	2(Left)	$Q_V^{\text{neu}}, Q_A^{\text{neu}}$	$\mathcal{D}_{\text{neut}}$
SFF	1(Left)	$Q_S^{\text{neu}}, Q_P^{\text{neu}}$	$\mathcal{D}_{\text{neut}}$
FVV	2(Right)	$Q_V^{\text{ch}}, Q_A^{\text{ch}}$	\mathcal{D}_{ch}
FSS	1(Right)	$Q_S^{\text{ch}}, Q_P^{\text{ch}}$	\mathcal{D}_{ch}

Table 5: Topology assignment to each contribution to a_μ in the unitary gauge [25]

The denominator \mathcal{D} from (67) depends on whether the diagram has a neutral or charged boson exchange:

$$\mathcal{D}_{\text{neut}}(x, \epsilon, \lambda) = (1-x)(1-\lambda^2 x) + \epsilon^2 \lambda^2 x, \quad (68)$$

$$\mathcal{D}_{\text{ch}}(x, \epsilon, \lambda) = (\epsilon\lambda)^2 (1-x) \left(1 - \frac{x}{\epsilon^2}\right) + x. \quad (69)$$

For the neutral exchange topologies (VFF and SFF), the numerator $Q_X(x, \epsilon, \lambda)$ in (67) is given by

$$\begin{aligned} Q_S^{\text{neut}} &= x^2 (1 + \epsilon - x), \\ Q_P^{\text{neut}} &= x^2 (1 - \epsilon - x), \\ Q_V^{\text{neut}} &= 2x(1-x)(x - 2(1-\epsilon)) + \lambda^2 (1-\epsilon)^2 x^2 (1 + \epsilon - x), \\ Q_A^{\text{neut}} &= 2x(1-x)(x - 2(1+\epsilon)) + \lambda^2 (1+\epsilon)^2 x^2 (1 - \epsilon - x). \end{aligned}$$

For the charged exchange topologies (FVV and FSS):

$$\begin{aligned} Q_S^{\text{ch}} &= -x(1-x)(x + \epsilon), \\ Q_P^{\text{ch}} &= -x(1-x)(x - \epsilon), \\ Q_V^{\text{ch}} &= 2x^2(1+x-2\epsilon) + \lambda^2 (1-\epsilon)^2 x(1-x)(x + \epsilon), \\ Q_A^{\text{ch}} &= 2x^2(1+x+2\epsilon) + \lambda^2 (1+\epsilon)^2 x(1-x)(x - \epsilon). \end{aligned}$$

So, VFF (V neutral boson) contribution to a_μ is given by

$$a_\mu(\text{VFF}) = \frac{m_\mu^2}{8\pi^2 M_B^2} \left[|C_V|^2 \mathcal{L}_V^{\text{neut}}(\epsilon, \lambda) + |C_A|^2 \mathcal{L}_A^{\text{neut}}(\epsilon, \lambda) \right]$$

with

$$\mathcal{L}_{V,A}^{\text{neut}}(\epsilon, \lambda) = \int_0^1 \frac{Q_{V,A}^{\text{neu}}(x, \epsilon, \lambda)}{\mathcal{D}^{\text{neu}}(x, \epsilon, \lambda)} dx.$$

The topology assignment formulae is summarized in Table 5.

References

- [1] Jogesh C. Pati and Abdus Salam. Lepton number as the fourth "color". *Phys. Rev. D*, 10:275–289, Jul 1974.
- [2] R. N. Mohapatra and J. C. Pati. "natural" left-right symmetry. *Phys. Rev. D*, 11:2558–2561, May 1975.
- [3] Rabindra N. Mohapatra and Jogesh C. Pati. Left-right gauge symmetry and an "isoconjugate" model of CP violation. *Phys. Rev. D*, 11:566–571, Feb 1975.
- [4] G. Senjanovic and R. N. Mohapatra. Exact left-right symmetry and spontaneous violation of parity. *Phys. Rev. D*, 12:1502–1505, Sep 1975.
- [5] Goran Senjanović. Spontaneous breakdown of parity in a class of gauge theories. *Nuclear Physics B*, 153:334–364, 1979.
- [6] Rabindra N. Mohapatra. Mechanism for understanding small neutrino mass in superstring theories. *Phys. Rev. Lett.*, 56:561–563, Feb 1986.

- [7] P. S. Bhupal Dev and R. N. Mohapatra. TeV Scale Inverse Seesaw in SO(10) and Leptonic Non-Unitarity Effects. *Phys. Rev. D*, 81:013001, 2010.
- [8] Wai-Yee Keung and Goran Senjanović. Majorana neutrinos and the production of the right-handed charged gauge boson. *Phys. Rev. Lett.*, 50:1427–1430, May 1983.
- [9] S. Bertolini, J. O. Eeg, A. Maiezza, and F. Nesti. New physics in ε' from chromomagnetic contributions and limits on left-right symmetry. *Phys. Rev. D*, 86:095013, Nov 2012.
- [10] Stefano Bertolini, Alessio Maiezza, and Fabrizio Nesti. Present and Future K and B Meson Mixing Constraints on TeV Scale Left-Right Symmetry. *Phys. Rev. D*, 89(9):095028, 2014.
- [11] G. W. Bennett and et. al. Final report of the e821 muon anomalous magnetic moment measurement at bnl. *Phys. Rev. D*, 73:072003, Apr 2006.
- [12] B. Abi and et. al. Measurement of the positive muon anomalous magnetic moment to 0.46 ppm. *Phys. Rev. Lett.*, 126:141801, Apr 2021.
- [13] D. P. Aguillard and et. al. Measurement of the positive muon anomalous magnetic moment to 0.20 ppm. *Phys. Rev. Lett.*, 131:161802, Oct 2023.
- [14] D. P. Aguillard et al. Measurement of the Positive Muon Anomalous Magnetic Moment to 127 ppb. *Phys. Rev. Lett.*, 135(10):101802, 2025.
- [15] R. Aliberti et. al. The anomalous magnetic moment of the muon in the standard model: an update. *Physics Reports*, 1143:1–158, 2025. The anomalous magnetic moment of the muon in the Standard Model: An update.
- [16] Peter Athron, Kilian Möhling, Dominik Stöckinger, and Hyejung Stöckinger-Kim. The muon magnetic moment and physics beyond the standard model. *Prog. Part. Nucl. Phys.*, 148:104225, 2026.
- [17] Chris Kelso, H. N. Long, R. Martinez, and Farinaldo S. Queiroz. Connection of $g - 2_\mu$, electroweak, dark matter, and collider constraints on 331 models. *Phys. Rev. D*, 90:113011, Dec 2014.
- [18] J. S. Alvarado, S. F. Mantilla, R. Martinez, F. Ochoa, and Cristian Sierra. Gauged nonuniversal $u(1)_X$ model to study muon $g - 2$ and b meson anomalies. *Phys. Rev. D*, 108:095040, Nov 2023.
- [19] Pei-Hong Gu and Utpal Sarkar. Leptogenesis with Linear, Inverse or Double Seesaw. *Phys. Lett. B*, 694:226–232, 2011.
- [20] Vedran Brdar and Alexei Yu Smirnov. Low Scale Left-Right Symmetry and Naturally Small Neutrino Mass. *JHEP*, 02:045, 2019.
- [21] M. E. Catano, R Martinez, and F. Ochoa. Neutrino masses in a 331 model with right-handed neutrinos without doubly charged Higgs bosons via inverse and double seesaw mechanisms. *Phys. Rev. D*, 86:073015, 2012.
- [22] A. G. Dias, C. A. de S. Pires, P. S. Rodrigues da Silva, and A. Sampieri. Simple realization of the inverse seesaw mechanism. *Phys. Rev. D*, 86:035007, Aug 2012.
- [23] J. A. Casas and A. Ibarra. Oscillating neutrinos and $\mu \rightarrow e, \gamma$. *Nucl. Phys. B*, 618:171–204, 2001.
- [24] E. Arganda, M. J. Herrero, X. Marcano, and C. Weiland. Imprints of massive inverse seesaw model neutrinos in lepton flavor violating higgs boson decays. *Phys. Rev. D*, 91:015001, Jan 2015.
- [25] Fred Jegerlehner and Andreas Nyffeler. The muon $g - 2$. *Physics Reports*, 477(1):1–110, 2009.
- [26] Ivan Esteban, M. C. Gonzalez-Garcia, Michele Maltoni, Ivan Martinez-Soler, João Paulo Pinheiro, and Thomas Schwetz. NuFit-6.0: updated global analysis of three-flavor neutrino oscillations. *JHEP*, 12:216, 2024.